This document is the accepted manuscript version of the following article:
Pieber, S. M., El Haddad, I., Slowik, J. G., Canagaratna, M. R., Jayne, J. T., Platt, S. M., … Prévôt, A. S. H. (2016). Inorganic salt interference on CO2+ in aerodyne AMS and ACSM organic aerosol composition studies. Environmental Science and Technology, 50(19), 10494-10503. https://doi.org/10.1021/acs.est.6b01035

Inorganic salt interference on CO_2^+ in Aerodyne AMS and ACSM organic aerosol composition studies.

Simone M. Pieber[1], Imad El Haddad[1], Jay G. Slowik[1,*], Manjula R. Canagaratna[2], John T. Jayne[2], Stephen M. Platt[1,5], Carlo Bozzetti[1], Kaspar R. Daellenbach[1], Roman Fröhlich[1], Athanasia Vlachou[1], Felix Klein[1], Josef Dommen[1], Branka Miljevic[3], Jose L. Jimenez[4], Douglas R. Worsnop[2], Urs Baltensperger[1], André S. H. Prévôt[1,*]

[1]Paul Scherrer Institute, Laboratory of Atmospheric Chemistry, CH-5232 Villigen, Switzerland

[2]Aerodyne Research, Inc., Billerica, MA, USA

[3]Queensland University of Technology, Brisbane, Australia

[4]Department of Chemistry & Biochemistry and CIRES, University of Colorado, Boulder, CO, USA

[5]Now at Norwegian Institute for Air Research, PO Box 100, 2027 Kjeller, Norway

*correspondence to: e-mail: andre.prevot@psi.ch; phone: +41 56 310 4202,
e-mail: jay.slowik@psi.ch. ; phone: +41 56 310 5755

address: Paul Scherrer Institute, Laboratory of Atmospheric Chemistry, OFLA/004, CH-5232 Villigen, Switzerland

Abstract

The Aerodyne aerosol mass spectrometer (AMS) and Aerodyne aerosol chemical speciation monitor (ACSM) mass spectral fingerprints are widely used to determine organic aerosol (OA) elemental composition and oxidation state, and to quantify OA sources. The OA CO_2^+ fragment is among the most important measurements for such analyses. Here, we show that a non-particle bound CO_2^+ signal can arise from reactions on the particle vaporizer and/or ion chamber induced by thermal decomposition products of inorganic salts. In our tests (8 instruments, n=29) ammonium nitrate (NH_4NO_3) causes a median CO_2^+ interference signal of +3.4% relative to nitrate, and is highly variable among instruments and with measurement history (percentiles P_{10-90}=+0.4 to +10.2%). Other semi-refractory nitrate salts showed 2-10 times enhanced interference compared to NH_4NO_3, while the ammonium sulfate ($(NH_4)_2SO_4$) induced interference was 3-10 times lower. As the CO_2^+ interference is propagated to other mass spectral ions, it affects the calculated OA mass, mass spectra, molecular oxygen-to-carbon (O:C) ratio and f_{44}. The resulting bias may be trivial for most ambient datasets, but can be significant for aerosol with higher inorganic fractions (>50%), e.g. at low ambient temperatures, or in laboratory experiments. The large inter-instrument variation makes it imperative to regularly monitor the extent of this effect on individual AMS/ACSM systems.

TOC Graphic

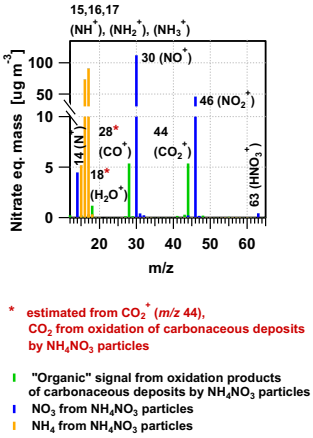

Graphical Abstract (TOC).

Introduction

Aerosol climate[1] and health[2] effects depend on many parameters, including particle size and chemical composition. Organic aerosol (OA) is often a large fraction of the total ambient aerosol mass, with highly variable properties and sources.[3] Its chemical composition, especially the oxidation state, is a key parameter for the description of OA volatility[4], hygroscopicity[5] and atmospheric processing[3].

The Aerodyne aerosol mass spectrometer[6-8] (AMS) and the aerosol chemical speciation monitor[9, 10] (ACSM) permit simultaneous quantification of ammonium nitrate (NH_4NO_3), ammonium sulfate ($(NH_4)_2SO_4$), ammonium chloride (NH_4Cl) and OA mass in sub-micron aerosol in real-time. OA mass spectra provide valuable information on the degree of oxygenation of organic species and are used extensively in factor analysis to quantify primary vs secondary organic aerosol sources (SOA).[11] SOA is typically captured by one or more oxygenated organic aerosol (OOA) factors which are characterized by different fractional contribution of the CO_2^+ fragment at *m/z* 44 (f_{44}) a surrogate for organic acids and therefore aged aerosols.[5, 8, 11, 13] The effect of the CO_2^+ fragment is further amplified in total OA mass and molecular oxygen-to-carbon (O:C) calculations, because it is used to estimate the intensities of several other related OOA fragments, such as CO^+ and H_2O^+.[12, 13] Therefore, the accurate measurement of the CO_2^+ fragment is important for OA quantification, estimations of bulk elemental composition and properties, such as O:C ratio[14] and f_{44}-f_{43} relationship[15], and source apportionment.

AMS/ACSM instruments impact and flash-vaporize a focused particle beam in a high vacuum onto an inverted cone-shaped porous tungsten vaporizer, typically heated to 600 °C [8, 16] to generate vapors that can undergo electron ionization and mass spectral classification. When applied to heterogeneous mixtures of chemical constituents, the flash-vaporization technique may be sensitive to memory or matrix effects. For example,instrument-to-instrument variability of especially f_{44} was recently indicated in an inter-comparison of 14 quadrupole (Q)-ACSMs, 1 high resolution time-of-flight (HR-ToF)-ACSM and 1 HR-ToF-AMS for ambient winter time aerosol in Paris.[19, 20] The observed variability is interpreted as instrument-dependent degree of pyrolysis and species dependent evaporation time scales in the samples, and is currently under further investigations (publication forthcoming). While no matrix effects between inorganic species and organic/inorganic mixtures were observed in the above mentioned inter-comparison[19, 20] and other studies[17, 18, 21], the direct interactions of particles with the vaporizer, and small memory effects

were reported in the past.[16, 21, 22] Therefore, interactions of particles with the vaporizer and its surrounding ion chamber merit further investigations. Here we assess the effect of inorganic matrices on measured OA mass spectra. We focus, in particular, on the CO_2^+ fragment signal, and the impact that inorganic salts can have on the determination of OA mass and degree of oxidation in typical datasets.

Experimental

AMS/ACSM Instruments. 6 HR-ToF-AMS[7] (HR1-6), 1 compact-ToF-AMS[23] (CToF) and 1 Q-ACSM[10] (ACSM), all equipped with inverted cone-shaped porous tungsten vaporizers, were examined. The HR- and CToF-AMS provide quantitative size-resolved mass spectra of the non-refractory particle components. The particle beam is sampled through an aerodynamic lens and focused onto the heated porous tungsten vaporizer in high vacuum (10^{-5} Pa). The non-refractory particle components flash-vaporize and the resulting gas is ionized by electron ionization (EI) and classified in a mass spectrometer. We operated the instruments under standard conditions with a vaporizer temperature (T_{vap}) of 600 °C unless noted otherwise. Prior to flash-vaporization, the beam is either alternately blocked (*closed*) and unblocked (*open*), yielding particle mass spectra (MS mode) following subtraction of the two, or modulated by a spinning chopper wheel, yielding size-resolved spectra (PToF mode). Beam *open* and *closed* times are given in Table S1 (SI) for the conducted experiments; general switching times were 2.5 or 5 s for the HR instruments and 7.5 s for the CToF. Gas phase interferences are further accounted for by subtracting the signal during measurements of particle free sampling air. The Q-ACSM is limited to integer mass resolution and does not have a size resolution module, but provides quantitative mass spectra of the non-refractory aerosol, by alternately measuring the total and the filtered air. ACSM scans were recorded between *m/z* 10 and 149 at a scan rate of 200 ms amu^{-1} and the filter was switched after each scan, resulting in a switching time of 30 s. All data presented derive from open *minus* closed signals.

Experiments. Investigations were performed using laboratory aerosols generated (a) by nebulization of solutions, and (b) in smog chamber experiments (α-pinene (AP) SOA and NH_4NO_3). Analytical grade chemicals (Sigma-Aldrich, purity at least ≥ 98%) including NH_4NO_3, $(NH_4)_2SO_4$, NH_4Cl, sodium nitrate ($NaNO_3$), potassium nitrate (KNO_3), calcium nitrate ($Ca(NO_3)_2$), and isotopically labelled ammonium nitrate ($NH_4N^{18}O_3$, 95 atom-% ^{18}O), were studied. Ultra-pure water (18.2 MΩ cm, total organic carbon < 5 ppb, 25°C) was used. **a)**

Laboratory aerosol from high purity salts. The salts were dissolved in ultra-pure water and nebulized in a custom-built nebulizer using synthetic, CO_2-free air (N_2/O_2, 4.6) or argon (5.0) . The aerosol was dried and either sampled directly by the instruments, or passed through a bipolar charger and size selected with a differential mobility analyzer before sampling. Blank measurements with ultra-pure water were conducted identically.

b) Smog chamber (SC) experiments. To study the effect of NH_4NO_3 when mixed with OA, a series of experiments were performed in a 7 m^3 Teflon film SC: (i) pure α-pinene (AP) SOA (experiment HR3-ExptAP-1 to 3, Table S1-2), (ii) AP SOA mixed with NH_4NO_3 (HR3-ExptAP-AN-1 to 6), and (iii) pure NH_4NO_3 aerosol (HR3-Expt4/5) were investigated. Prior to each experiment the SC was reduced to a volume of 1 m^3, cleaned with O_3, water, and UV lights for 1 h, and thereafter flushed with dry clean air for 12 hours. For the AP SOA experiments, the SC was filled with humid air. Then (i) 30-40 ppb of AP were reacted with 300 ppb O_3. To study (ii) AP SOA mixed with NH_4NO_3 50 - 400 ppb NH_3 (6.0) was injected into the SC after all AP was reacted, followed by subsequent injections of HNO_3 to form internally mixed AP SOA/NH_4NO_3 particles. The HNO_3 was provided by nebulization of a diluted solution. Two experiments were conducted in which only pure NH_4NO_3 was formed in situ in the SC (iii). The SC was filled with humid air. Then, 200 ppb NH_3 and nebulized HNO_3were injected (HR3-Expt4). In the second experiment,HNO_3 was formed in situ by OH oxidation of NO_2 (HR3-Expt5).. 1 ppm NO_2 (1.8) and 300 ppb O_3 were injected. Nitrous acid (HONO) was prepared online according to Taira et al.[24], continuously flushed into the SC, and UV lights were turned on. Thereafter, 400 ppb NH_3 was injected to form NH_4NO_3. Particle phase instruments included an HR-ToF-AMS (HR3), a scanning mobility particle sizer and a condensation particle counter, all placed behind a Nafion dryer (RH behind dryer below 25%). A PTR-ToF-MS[25] was used to measure the concentrations of AP and d9-butanol, the decay of which is used as an OH tracer.[26]

Results and Discussion

Non-particle-bound CO_2^+ from NH_4NO_3. AMS/ACSM aerosol mass spectra of NH_4NO_3 - the most abundant form of inorganic nitrate in ambient aerosol - show CO_2^+ at *m/z* 44 (exact mass 43.9898), which cannot be explained by the main ions expected from the decomposition and fragmentation of NH_4NO_3, i.e. NH^+, NH_2^+, NH_3^+, NO^+, NO_2^+ and HNO_3^+(Fig. 1 and SI). A subset of tests conducted in argon to minimize the gas phase nitrogen background at *m/z* 28 reveals that

CO^+ is also observed. Additional unexpected ions were not detected above instrument background.

The observed CO_2^+ signal is directly proportional to the nitrate signal (denoted NO_3 to distinguish from the NO_3^+ ion (*m/z* 62) measured by the AMS/ACSM), which refers to the summed signal of all ions attributed to NO_3 following the standard fragmentation assumptions.[12, 13] CO_2^+ increases monotonically with increasing NH_4NO_3 concentrations (Eq. 1, Fig. S1, CO^+ shows similar trends as CO_2^+ but is not presented as only a limited number of tests were conducted in argon The magnitude of CO_2^+ relative to the anion signal is described by the slope *k* in Eq. 1. If a gas phase CO_2 background or any other constant source of CO_2 is not subtracted in this analysis, a non-zero intercept d is observed. However, this does not influence the determined *k*.

$$CO_2^+ = k \text{ anion signal} + d \qquad \text{Eq. 1}$$

To derive *k* for NH_4NO_3 the orthogonal distance linear fit is determined from CO_2^+ and NO_3 signals in nitrate equivalent mass (i.e. using a relative ionization efficiency of RIE=1).[8] This is equivalent to deriving *k* from ion counts in Hz.

CO_2^+ related to NH_4NO_3 sampling on the vaporizer is observed on all the tested instruments (6 HR, 1 CTOF and 1 ACSM), albeit the magnitude of *k* varies significantly between the tested instruments, and for a given instrument as a function of operation history. Our experiments (n=29 across 8 instruments) indicate a median, i.e. 50th percentile P_{50} of +3.4% (10th and 90th percentiles: $P_{10\text{-}90}$=+0.4 to +10.2%, Fig. 2a and Fig. S1). While HR4-6 (n=1-2) fall around the P_{10} estimate, the ACSM (n=1) falls above P_{75}. A wide spread of *k* as a function of measurement history is observed on instruments if monitored over a longer time period (HR1-3 as well as CTOF, for which data points spanning several years are available). Critically, these results show that an assumption of a single *k* for a given instrument or a standard *k* for all AMS/ACSM instruments is not warranted (further discussed below and in SI).

Carbonaceous species ("organic signal") including CO_2^+ (and CO^+) are generally detectable in the instrument background (*closed* mass spectra) even in the absence of active aerosol sampling. These signals are due to memory effects[21], and the slow release and thermal decomposition of semi-refractory residues deposited by particles on the 600 °C heated AMS/ACSM vaporizer and ion chamber walls. These deposited carbonaceous residues may include charred organic carbon (OC), elemental carbon (EC), and semi-refractory carbonates.

It is, in addition to contributing to the background signal, released as a consequence of reactions induced by thermal decomposition products of impinging NH_4NO_3 particles, leading to the rapid generation of CO_2 presented in the current study. As the instruments are exposed to varying levels and composition of aerosol over time, *k* varies with the instruments' memory. The relatively high *k* for the tested ACSM is thereby not surprising, due to longer sampling intervals on the vaporizer (typically 30 sec) compared to below 5 sec for AMS instruments, which favors memory effects (Fig. 2, Fig. S1, Fig. S2).

A contribution of particle-bound carbon or CO_2 in the aerosol source in our experiments is ruled out by using high purity chemicals, water and gases, along with simultaneous measurements on multiple instruments, and sampling of high purity NH_4NO_3 synthesized from gas phase precursors in a SC. However, other sources of carbon in the system might be impurities in the vaporizer material (99.9% porous tungsten, SI) itself as well as carbided tungsten filaments.[27]

Oxidation of organic carbonaceous residues to CO and CO_2 by HNO_3/NO_x is well known in mass spectrometry research of NO_2 and HNO_3.[27, 28] Soot oxidation research and the automobile industry make use of carbon oxidation under high NO_x conditions.[29-32] For instance, high NO_x levels and enhanced temperatures in the vehicle exhaust are used to facilitate regeneration of diesel particulate filters and to burn off carbonaceous deposits to CO_2. On the other hand, (elemental) carbon is used as a catalyst for the selective catalytic reduction of NO_x to N_2.[33-35] Likely, similar conditions drive the CO and CO_2 formation inside the ion chamber, when NH_4NO_3 or other nitrate salts decompose to HNO_3, NO_2 and NO (NO_x) on the 600 °C heated AMS/ACSM vaporizer. Also the observed CO^+/CO_2^+ ratio around 1 (note: EI impact CO^+/CO_2^+ ratio[36]=0.1) is in line with literature reports on soot oxidation with nitrogen oxides (0.2-1).[37] The fact that other small oxygenated fragments are not observed to similar extents is likely a result of induced surface oxidation of larger molecules The linear relationship observed between the CO_2^+ and NO_3 signal, and its evenly distributed fit residuals as a function of NO_3 concentration (Fig. S1f), imply that the CO_2 production follows first order reaction kinetics with respect to NO_3, where the actual oxidants (HNO_3/NO_x) are in turn proportional to NO_3.

Isotopically labelled ammonium nitrate ($NH_4N^{18}O_3$, 95 atom-% ^{18}O) was used to study the source of oxygen in the observed CO_2^+. The replacement of the ^{16}O isotope by an ^{18}O isotope in the NH_4NO_3 reduced the $C^{16}O_2^+$ observed at nominal *m/z* 44 at least by 40-70% (Fig. 2b). Contributions to $C^{16}O^{18}O^+$ (*m/z* 45.9940) and $C^{18}O_2^+$ (*m/z* 47.9983) could not be directly estimated, due to peak overlap and thereby potential contributions of $N^{16}O_2^+$ (*m/z* 45.9929) and

$N^{16}O^{18}O^+$ (*m/z* 47.9971). The reduction at *m/z* 44 confirms our hypothesis that a significant part of the CO_2^+ arises from the reactions of HNO_3/NO_x with deposited refractory carbonaceous matter (charred OC or genuine EC). The remaining $C^{16}O_2^+$ (30-60%) in these labelled experiments can arise from oxygen in the previously deposited carbonaceous material (e.g. OC and oxidized EC). Alternatively, deposited carbonates may release CO_2 upon reaction with HNO_3/NO_x, contributing to $C^{16}O_2^+$ in these experiments, and to CO_2 in normal operation (e.g. CO_2 release from $Ca(NO_3)_2$ upon reaction with HNO_3).[38] Likewise,[16]O impurities in the tungsten vaporizer material could contribute to the remaining $C^{16}O_2$. Drewnick et al.[16] showed recently that the contribution of gas phase $^{16}O_2$ for vaporizer-oxidation processes is negligible. Oxygen however facilitates carbon oxidation by NO_x[39] and the presence of gaseous O_2 in the instrument background during NH_4NO_3 sampling might therefore be another contributor to CO_2^+.

Non-particle-bound CO_2^+ from other salts. Non-particle-bound CO_2^+ is also induced by other salts, which decompose and give reactive species upon heating on the AMS/ACSM vaporizer (Fig. 2b). While *k* of CO_2^+ vs NO_3 is higher for KNO_3 (×2.5-4), $Ca(NO_3)_2$ (×4.5) and $NaNO_3$ (×3.5-11.5) on the tested instruments when compared to *k* of NH_4NO_3, *k* of CO_2^+ vs SO_4 is 3-10 times lower for $(NH_4)_2SO_4$ (×0.10-0.30). NH_4Cl did, as expected, not induce CO_2^+ formation in our experiments. Lower levels of CO_2^+ from $(NH_4)_2SO_4$ compared to that from NH_4NO_3 may result from a lower oxidative power of sulfur oxides compared to nitrogen oxides. Decomposition and fragmentation of the salts are presented in SI. Higher *k* for KNO_3, $Ca(NO_3)_2$ and $NaNO_3$ compared to that from NH_4NO_3 may result from semi-refractive behavior of those salts at 600 °C and the thereby enhanced interaction of reactive species (i.e. NO/NO_2, as HNO_3 does not form) when they thermally decompose (see discussion in SI).

Influence of aerosol properties on the interference. As discussed above, we show that *k* is independent of the NH_4NO_3 concentration (Fig. S1f). Further, it is independent of particle diameter (Fig. 3a). For mixed particles of AP SOA with NH_4NO_3, *k*, shows a similar magnitude as induced by pure NH_4NO_3 (Fig. 3b). This indicates that there are no significant additional matrix effects on the production of CO_2^+ for the system looked at (AP SOA/NH_4NO_3). We suggest therefore, that *k* is not affected by simultaneous presence of carbonaceous particles. Note that the intercept in Fig. 3b represents the particulate CO_2^+ contained in AP SOA (at NH_4NO_3=0).

Impact on organic aerosol mass and chemical composition measurements. To date, AMS/ACSM analyses have not considered the possibility of non-particle-bound CO_2^+ signal formed on the instrument vaporizer, and have instead classified this as particle-bound organic

mass. This can result in an overestimation of the organic mass at *m/z* 44 (Org_{44}). Additionally, CO_2^+-derived ion intensities and mass at *m/z* 28 (CO^+), 18 (H_2O^+), 17 (OH^+), 16 (O^+) and the associated isotopes are overestimated, when using standard fragmentation assumptions such as $Org_{28}=Org_{44}*1$, $Org_{18}=Org_{44}*0.225$, $Org_{17}=Org_{44}*0.05625$ and $Org_{16}=Org_{44}*0.009$.[12, 13]

As noted above, the NH_4NO_3 induced non-particle-bound CO_2^+ affects directly Org_{44}, and indirectly also Org_{18}, Org_{28}, to smaller extent Org_{17} and Org_{16}, and the associated isotopes, in standard data analysis routines.[12, 13] An example for an impacted data set is illustrated in Fig. 4, showing SOA formed from AP, and subsequently mixed with NH_4NO_3. SOA is formed from the reaction of AP with O_3 and OH radicals. The formed OA mass decays after reaching its peak due to particle wall losses. Subsequent injections of NH_3 and HNO_3 lead to mixing of OA with NH_4NO_3, introducing primarily an increase in the *m/z* 44 signal due to NH_4NO_3 induced non-particle-bound CO_2^+. The total OA mass, the mass spectrum and the f_{44}-f_{43} relationships are biased. Enhancements in other fragments, such as *m/z* 43 in these experiments, are assigned to collection efficiency changes due to mixing with NH_4NO_3 (detailed in the SI).

The magnitude of the bias introduced in ambient or laboratory data sets depends on multiple parameters. The (*i*) vaporizer's measurement history and (*ii*) the inorganic salts present (NH_4NO_3, $(NH_4)_2SO_4$, etc.) directly affect the relationship *k*. The (*iii*) mixing ratio of the inorganic salt to OA mass (e.g. NO_3/OA for NH_4NO_3) and (*iv*) the true f_{44}, O:C and H:C determine the extent of bias that a certain *k* will cause.

Fig. 5 presents estimations of the induced bias on (a) O:C and (b) H:C ratios, (c) f_{44}, and (d) OA mass for ambient (covering both summer and winter conditions) and laboratory data sets, using the percentiles of *k* (CO_2^+ vs NO_3) for NH_4NO_3 as determined on the investigated instruments (Fig. 2a, percentiles: P_{10}=+0.004, P_{25}=+0.019, P_{50}=+0.034, P_{75}=+0.064, P_{90}=+0.102). Note that these values reflect the specific instruments tested and should be interpreted as case studies rather than a statistically significant assessment of AMS/ACSM performance; individual instrument performance varies widely.

We assume three scenarios for the true particle composition in terms of O:C and H:C (see Fig. 5 caption). The associated f_{44} and organic matter (OM) / organic carbon (OC) content are estimated based on Canagaratna et al.[14]. Equations in SI.

Ratios of NH_4NO_3 (and other inorganic salts) to OA vary spatially and with diurnal or seasonal changes, as well as with variations in source activities. For example, high NH_4NO_3 contributions

to the total sub-micron aerosol have been reported during winter in Europe with NO_3/OA ~1.2 vs 0.1 for summer[3, 40-44], and for combustion emission studies, with ratios up to 10.[46, 47] Therefore, we span a NO_3/OA ratio of 0.1 – 10 in Fig. 5. Different ratios may also represent spatial differences between e.g. ammonia (NH_3) rich and poor regions.

Fig. 5 shows that for NO_3/OA=1 and our determined median NH_4NO_3 instrument interference (k=3.4%) the measured f_{44} would be overestimated by +20% at a true f_{44}=0.10, by +44% for f_{44}=0.05 and by +12% for f_{44}= 0.14. The median bias in f_{44} is not large enough to significantly affect the classification of the oxidized organic material as SV- and LV-OOA based on Ng et al.[15, 48] (SV-OOA: f_{44}=0.07±0.04, O:C=0.35±0.14; LV-OOA: f_{44}=0.17±0.04, O:C=0.73±0.14). However, instruments with k in our P_{10}-$_{90}$ range can lead to f_{44} biases from +1.6% to +117%. The higher end can shift the classification of oxidized aerosol from SV- to LV-OOA and also significantly bias O:C values for HR-AMS, and also when estimated from f_{44} in unit mass resolution AMS/ACSM spectra[12,14]. For the other parameters, the bias observed for a P_{50} k is estimated to be +7.8% (P_{10-90}=+0.7-+37%) for O:C, +6.2% (P_{10-90}=+0.8-+18%) for OA mass, and -3.3% (P_{10-90} -0.4 to -10.4%) for H:C. The P_{50} biases are mostly within the uncertainties for O:C and H:C estimations by Canagaratna et al.[14] (28% and 13% respectively) and for OA mass by Bahreini et al. (38%)[49].Combustion emissions yield a complex mix of organic and inorganic components in the submicron particle phase. The inorganic material is either emitted directly (ash components in solid fuel combustion), or formed via secondary processes (for instance NH_4NO_3 and $(NH_4)_2SO_4$). As example, recent gasoline vehicles are equipped with three-way catalysts, which can emit NH_3, due to over-reduction of NO_x in the exhaust.[50, 51] Upon ageing, particulate NH_4NO_3 is formed as a secondary compound, and may by far exceed the formation of SOA. Ratios up to 10 and more NO_3/OA have been observed when testing gasoline vehicle exhaust in smog chambers.[46, 47] At an NO_3/OA=5, , a P_{50} k results in a bias of +82% on the f_{44} (P_{10-90}=+7.8 to ~ +360%), along with a P_{50}=+31% bias for the OA mass (P_{10-90}=+4.0-+92%), and +34% on the O:C (+4-+133%). This would shift a true O:C=0.50 to O:C=0.67. In fact, unexpectedly high O:C ratios of 0.7 and higher have been previously reported for vehicle emission aging studies.[45] A maximum bias on the H:C under these mixing conditions is -37% (P_{90}).

Sulfuric acid and $(NH_4)_2SO_4$ are formed in emission plumes from coal combustion or marine fuel combustion in ship engines, and may be present at relatively high concentrations under those conditions. $(NH_4)_2SO_4$ is also frequently used as seed aerosol in smog chamber experiments. An estimated bias on f_{44} from $(NH_4)_2SO_4$ interference at relevant SO_4/OA ratios for ambient

observations (0.5-2)[3, 52] spans from +1.6% and +23% at a P_{50} interference for k (CO_2^+ vs SO_4)=0.007. The upper estimation at SO_4/OA=2 (P_{90}) is +63%. The respective P_{90} bias is +9.2% for OA mass, +19% on the O:C and -5.5% on the H:C ratio (Fig. S5).

During measurements of ambient aerosol, NH_4NO_3 and $(NH_4)_2SO_4$ are the dominant inorganic species detected with AMS/ACSM.[3] Other salts ($NaNO_3$, KNO_3, $Ca(NO_3)_2$) with enhanced interference k under standard measurement conditions can introduce significant biases already at lower mixing ratios and may be relevant in particular environments. Examples are areas with marine aerosols, when NaCl partially or fully reacts with NO_x/HNO_3 to form $NaNO_3$. Such particles are mostly in the super micron mode and are sampled very inefficiently by the AMS/ACSM.[53] However, the presence of $NaNO_3$ as well as inorganic dust containing nitrate and sulfate salts may become more critical when a $PM_{2.5}$ inlet lens[54] is used in combination with the AMS. $NaNO_3$ or similar salts may also be used when studying effects of mixing organic and inorganic aerosol mass, and could lead to biases as well in laboratory studies, especially if relatively low OA concentrations were used. Ash components from solid fuel combustion may include KNO_3 or potassium sulfate (K_2SO_4).[55, 56]

Finally, CO^+ (*m/z* 28) cannot be detected directly under typical operating conditions due to interference from the N_2^+ signal. Therefore, as long as the CO^+ signal is estimated from CO_2^+, as in the standard data analysis routine, additional non-particle-bound CO^+ does not cause an additional interference in the mass spectra and derived parameters. In laboratory experiments conducted in a different atmosphere (e.g. argon) that allows estimating e.g. CO^+ from the raw mass spectrum, however, a potential influence on other signals needs to be accounted for.

Implications. NH_4NO_3 and other nitrate salts, as well as $(NH_4)_2SO_4$, can lead to formation of CO and CO_2 on the Aerodyne AMS/ACSM vaporizers, as they thermally decompose to reactive species that can induce release of (otherwise refractory) carbonaceous material already present in the instrument. The observed interference introduces biases in OA mass and chemical composition measurements, particularly regarding the aerosol oxygen content (f_{44}, O:C).

The bias is a function of the interference k and the particle composition (inorganic fraction and oxidation state). Based on the magnitude k of the interference estimated from our tests on 8 instruments (6 HR, 1 CTOF and 1 ACSM), which yielded a median of +3.4% across all tests, we estimate that the bias will be small (less than a few percent) for most ambient data. This is supported by the fact that NH_4NO_3 fractions are typically low compared to OA, and $(NH_4)_2SO_4$

(globally equal to OA) is less efficient in CO_2 formation. However, the bias can become significant in particular environments (chamber experiments with inorganic seed aerosols or gasoline vehicle exhaust ageing), periods of high inorganic mass fractions (e.g. European winter), specific ambient research questions (e.g. investigating temporal or spatial different aerosol compositions), or for instruments with poor vaporizer conditions. For example a *k* above our determined median 3.4% at NO_3/OA=1, or a *k* of 10.2% at NO_3/OA = 0.1-0.2 cause biases that exceed limits to impact f_{44}-f_{43}-derived SV- and LV-OOA splits[15, 48], or the uncertainties for O:C, H:C and OA mass estimations. [14,49] Therefore, the interference need to be calibrated for in the analyses and interpretation of the data.

We suggest including the introduced bias in the error estimation, after careful determination of the relationship *k* for the relevant salts. For sampling conditions with large bias, data should be corrected by subtracting the interference signal. An example on how to do this by linking *k* to the inorganic signal using the AMS/ACSM standard data analysis procedures and fragmentation table is provided in SI.

As *k* is not constant across different instruments and will also vary over measurement time for a given instrument depending on the level of exposure to aerosol and its composition, careful and frequent determination of the relationship *k* between the CO_2^+ and anion signal are crucial. This should be done with aerosol generated under clean conditions and with typical instrument settings used for data collection. The standard calibrations regularly performed for the determination of NO_3 ionization efficiency and NH_4 and SO_4 relative ionization efficiency offer such an opportunity.

Previous interpretations of OA oxygen content and related chemical and physical aerosol properties that were made based on (i) simple comparison of f_{44}- f_{43} or (ii) AMS/ACSM derived O:C and H:C, as well the (iii) interpretation of the AMS/ACSM *m/z* 44 signal as organic acid derived, need to be discussed with precaution by taking into account the possible impact of the interference. Calibration mass spectra from each experiment can be used to retrospectively diagnose *k* for a given instrument and time period.

Acknowledgements

We would like to thank the AMS/ACSM-users community and members from the Laboratory of Atmospheric Chemistry, especially Emily Bruns, Francesco Canonaco, Miriam Elser, Maarten

Heringa, Lisa Pfaffenberger and Robert Wolf for fruitful discussions on their ionization efficiency calibration data to help us understand the observed instrument interferences. SMP acknowledges support from the SNF (WOOSHI, 140590). JGS acknowledges support from the SNF (starting grant BSSGI0_155846). MRC, JTJ, and DRW acknowledge support from EPA (EP-04-008) and DoE (DE-SC0001673). JLJ was supported by NSF AGS-1360834 and NASA NNX15AH33A/ NNX15AT96G.

Supporting Information Available

Supporting Information is available as noted in the text. This information is available free of charge via the Internet at http://pubs.acs.org.

References

1. IPCC, Contribution of Working Group I to the Fifth Assessment Report of the Intergovernmental Panel on Climate Change. In Cambridge University Press: 2013.
2. Dockery, D. W.; Pope, C. A.; Xu, X.; Spengler, J. D.; Ware, J. H.; Fay, M. E.; Ferris, B. G.; Speizer, F. E., An Association between Air Pollution and Mortality in Six U.S. Cities. *New England Journal of Medicine* **1993,** *329*, (24), 1753-1759.
3. Jimenez, J. L.; Canagaratna, M. R.; Donahue, N. M.; Prevot, A. S. H.; Zhang, Q.; Kroll, J. H.; DeCarlo, P. F.; Allan, J. D.; Coe, H.; Ng, N. L.; Aiken, A. C.; Docherty, K. S.; Ulbrich, I. M.; Grieshop, A. P.; Robinson, A. L.; Duplissy, J.; Smith, J. D.; Wilson, K. R.; Lanz, V. A.; Hueglin, C.; Sun, Y. L.; Tian, J.; Laaksonen, A.; Raatikainen, T.; Rautiainen, J.; Vaattovaara, P.; Ehn, M.; Kulmala, M.; Tomlinson, J. M.; Collins, D. R.; Cubison, M. J.; Dunlea, E. J.; Huffman, J. A.; Onasch, T. B.; Alfarra, M. R.; Williams, P. I.; Bower, K.; Kondo, Y.; Schneider, J.; Drewnick, F.; Borrmann, S.; Weimer, S.; Demerjian, K.; Salcedo, D.; Cottrell, L.; Griffin, R.; Takami, A.; Miyoshi, T.; Hatakeyama, S.; Shimono, A.; Sun, J. Y.; Zhang, Y. M.; Dzepina, K.; Kimmel, J. R.; Sueper, D.; Jayne, J. T.; Herndon, S. C.; Trimborn, A. M.; Williams, L. R.; Wood, E. C.; Middlebrook, A. M.; Kolb, C. E.; Baltensperger, U.; Worsnop, D. R., Evolution of organic aerosols in the atmosphere. *Science* **2009,** *326*, (5959), 1525-1529.
4. Kroll, J. H.; Donahue, N. M.; Jimenez, J. L.; Kessler, S. H.; Canagaratna, M. R.; Wilson, K. R.; Altieri, K. E.; Mazzoleni, L. R.; Wozniak, A. S.; Bluhm, H.; Mysak, E. R.; Smith, J. D.; Kolb, C. E.; Worsnop, D. R., Carbon oxidation state as a metric for describing the chemistry of atmospheric organic aerosol. *Nat Chem* **2011,** *3*, (2), 133-139.
5. Duplissy, J.; De Carlo, P. F.; Dommen, J.; Alfarra, M. R.; Metzger, A.; Barmpadimos, I.; Prevot, A. S. H.; Weingartner, E.; Tritscher, T.; Gysel, M.; Aiken, A. C.; Jimenez, J. L.; Canagaratna, M. R.; Worsnop, D. R.; Collins, D. R.; Tomlinson, J.; Baltensperger, U., Relating hygroscopicity and composition of organic aerosol particulate matter. *Atmos. Chem. Phys.* **2011,** *11*, (3), 1155-1165.
6. Jayne, J. T.; Leard, D. C.; Zhang, X.; Davidovits, P.; Smith, K. A.; Kolb, C. E.; Worsnop, D. R., Development of an aerosol mass spectrometer for size and composition analysis of submicron particles. *Aerosol Sci. Technol.* **2000,** *33*, (1-2), 49-70.
7. DeCarlo, P. F.; Kimmel, J. R.; Trimborn, A.; Northway, M. J.; Jayne, J. T.; Aiken, A. C.; Gonin, M.; Fuhrer, K.; Horvath, T.; Docherty, K. S.; Worsnop, D. R.; Jimenez, J. L., Field-deployable, high-resolution, time-of-flight aerosol mass spectrometer. *Anal. Chem.* **2006,** *78*, (24), 8281-8289.
8. Canagaratna, M. R.; Jayne, J. T.; Jimenez, J. L.; Allan, J. D.; Alfarra, M. R.; Zhang, Q.; Onasch, T. B.; Drewnick, F.; Coe, H.; Middlebrook, A., Chemical and microphysical characterization of ambient aerosols with the Aerodyne aerosol mass spectrometer. *Mass Spectrom Rev* **2007,** *26*, (2), 185-222.

9. Fröhlich, R.; Cubison, M. J.; Slowik, J. G.; Bukowiecki, N.; Prévôt, A. S. H.; Baltensperger, U.; Schneider, J.; Kimmel, J. R.; Gonin, M.; Rohner, U.; Worsnop, D. R.; Jayne, J. T., The ToF-ACSM: A portable aerosol chemical speciation monitor with TOFMS detection. *Atmos. Meas. Tech.* **2013,** *6*, (11), 3225-3241.
10. Ng, N. L.; Herndon, S. C.; Trimborn, A.; Canagaratna, M. R.; Croteau, P. L.; Onasch, T. B.; Sueper, D.; Worsnop, D. R.; Zhang, Q.; Sun, Y. L.; Jayne, J. T., An Aerosol Chemical Speciation Monitor (ACSM) for routine monitoring of the composition and mass concentrations of ambient aerosol. *Aerosol Sci. Technol.* **2011,** *45*, (7), 770-784.
11. Zhang, Q.; Jimenez, J. L.; Canagaratna, M. R.; Allan, J. D.; Coe, H.; Ulbrich, I.; Alfarra, M. R.; Takami, A.; Middlebrook, A. M.; Sun, Y. L.; Dzepina, K.; Dunlea, E. J.; Docherty, K. S.; DeCarlo, P. F.; Salcedo, D.; Onasch, T.; Jayne, J.; Miyoshi, T.; Shimono, A.; Hatakeyama, S.; Takegawa, N.; Kondo, Y.; Schneider, J.; Drewnick, F.; Borrmann, S.; Weimer, S.; Demerjian, K.; Williams, P. I.; Bower, K.; Bahreini, R.; Cottrell, L.; Griffin, R.; Rautiainen, J.; Sun, J. Y.; Zhang, Y. M.; Worsnop, D., Ubiquity and dominance of oxygenated species in organic aerosols in anthropogenically-influenced Northern Hemisphere mid latitudes. *Geophys. Res. Lett.* **2007,** *34*, (13), L13801.
12. Aiken, A. C.; Decarlo, P. F.; Kroll, J. H.; Worsnop, D. R.; Huffman, J. A.; Docherty, K. S.; Ulbrich, I. M.; Mohr, C.; Kimmel, J. R.; Sueper, D.; Sun, Y.; Zhang, Q.; Trimborn, A.; Northway, M.; Ziemann, P. J.; Canagaratna, M. R.; Onasch, T. B.; Alfarra, M. R.; Prevot, A. S. H.; Dommen, J.; Duplissy, J.; Metzger, A.; Baltensperger, U.; Jimenez, J. L., O/C and OM/OC ratios of primary, secondary, and ambient organic aerosols with high-resolution time-of-flight aerosol mass spectrometry. *Environ. Sci. Technol.* **2008,** *42*, (12), 4478-4485.
13. Allan, J. D.; Delia, A. E.; Coe, H.; Bower, K. N.; Alfarra, M. R.; Jimenez, J. L.; Middlebrook, A. M.; Drewnick, F.; Onasch, T. B.; Canagaratna, M. R.; Jayne, J. T.; Worsnop, D. R., A generalised method for the extraction of chemically resolved mass spectra from Aerodyne aerosol mass spectrometer data. *J. Aerosol Sci.* **2004,** *35*, (7), 909-922.
14. Canagaratna, M. R.; Jimenez, J. L.; Kroll, J. H.; Chen, Q.; Kessler, S. H.; Massoli, P.; Hildebrandt Ruiz, L.; Fortner, E.; Williams, L. R.; Wilson, K. R.; Surratt, J. D.; Donahue, N. M.; Jayne, J. T.; Worsnop, D. R., Elemental ratio measurements of organic compounds using aerosol mass spectrometry: Characterization, improved calibration, and implications. *Atmos. Chem. Phys.* **2015,** *15*, (1), 253-272.
15. Ng, N. L.; Canagaratna, M. R.; Zhang, Q.; Jimenez, J. L.; Tian, J.; Ulbrich, I. M.; Kroll, J. H.; Docherty, K. S.; Chhabra, P. S.; Bahreini, R.; Murphy, S. M.; Seinfeld, J. H.; Hildebrandt, L.; Donahue, N. M.; Decarlo, P. F.; Lanz, V. A.; Prévôt, A. S. H.; Dinar, E.; Rudich, Y.; Worsnop, D. R., Organic aerosol components observed in Northern Hemispheric datasets from Aerosol Mass Spectrometry. *Atmos. Chem. Phys.* **2010,** *10*, (10), 4625-4641.
16. Drewnick, F.; Diesch, J. M.; Faber, P.; Borrmann, S., Aerosol mass spectrometry: particle–vaporizer interactions and their consequences for the measurements. *Atmos. Meas. Tech.* **2015,** *8*, (9), 3811-3830.
17. Matthew, B. M.; Middlebrook, A. M.; Onasch, T. B., Collection efficiencies in an aerodyne aerosol mass spectrometer as a function of particle phase for laboratory generated aerosols. *Aerosol Sci. Technol.* **2008,** *42*, (11), 884-898.
18. Hogrefe, O.; Drewnick, F.; Lala, G. G.; Schwab, J. J.; Demerjian, K. L., Development, Operation and Applications of an Aerosol Generation, Calibration and Research Facility Special Issue of Aerosol Science and Technology on Findings from the Fine Particulate Matter Supersites Program. *Aerosol Sci. Technol.* **2004,** *38*, (sup1), 196-214.
19. Fröhlich, R.; Crenn, V.; Setyan, A.; Belis, C. A.; Canonaco, F.; Favez, O.; Riffault, V.; Slowik, J. G.; Aas, W.; Aijälä, M.; Alastuey, A.; Artiñano, B.; Bonnaire, N.; Bozzetti, C.; Bressi, M.; Carbone, C.; Coz, E.; Croteau, P. L.; Cubison, M. J.; Esser-Gietl, J. K.; Green, D. C.; Gros, V.; Heikkinen, L.; Herrmann, H.; Jayne, J. T.; Lunder, C. R.; Minguillón, M. C.; MoÄnik, G.; O'Dowd, C. D.; Ovadnevaite, J.; Petralia, E.; Poulain, L.; Priestman, M.; Ripoll, A.; Sarda-Estève, R.; Wiedensohler, A.; Baltensperger, U.; Sciare, J.; Prévôt, A. S. H., ACTRIS ACSM intercomparison - Part 2: Intercomparison of ME-2 organic source apportionment results from 15 individual, co-located aerosol mass spectrometers. *Atmos. Meas. Tech.* **2015,** *8*, (6), 2555-2576.
20. Crenn, V.; Sciare, J.; Croteau, P. L.; Verlhac, S.; Fröhlich, R.; Belis, C. A.; Aas, W.; Äijälä, M.; Alastuey, A.; Artiñano, B.; Baisnée, D.; Bonnaire, N.; Bressi, M.; Canagaratna, M.; Canonaco, F.; Carbone, C.; Cavalli, F.; Coz, E.; Cubison, M. J.; Esser-Gietl, J. K.; Green, D. C.; Gros, V.; Heikkinen, L.;

Herrmann, H.; Lunder, C.; Minguillón, M. C.; Močnik, G.; O'Dowd, C. D.; Ovadnevaite, J.; Petit, J. E.; Petralia, E.; Poulain, L.; Priestman, M.; Riffault, V.; Ripoll, A.; Sarda-Estève, R.; Slowik, J. G.; Setyan, A.; Wiedensohler, A.; Baltensperger, U.; Prévôt, A. S. H.; Jayne, J. T.; Favez, O., ACTRIS ACSM intercomparison – Part I: Reproducibility of concentration and fragment results from 13 individual Quadrupole Aerosol Chemical Speciation Monitors (Q-ACSM) and consistency with Time-of-Flight ACSM (ToF-ACSM), High Resolution ToF Aerosol Mass Spectrometer (HR-ToF-AMS) and other co-located instruments. *Atmos. Meas. Tech. Discuss.* **2015,** *8*, (7), 7239-7302.

21. Drewnick, F.; Hings, S. S.; Alfarra, M. R.; Prevot, A. S. H.; Borrmann, S., Aerosol quantification with the Aerodyne Aerosol Mass Spectrometer: Detection limits and ionizer background effects. *Atmos. Meas. Tech.* **2009,** *2*, (1), 33-46.

22. Jimenez, J. L.; Bahreini, R.; Cocker, D. R.; Zhuang, H.; Varutbangkul, V.; Flagan, R. C.; Seinfeld, J. H.; O'Dowd, C. D.; Hoffmann, T., New particle formation from photooxidation of diiodomethane (CH2I2). *J. Geophys. Res. D Atmos.* **2003,** *108*, (D10), n/a-n/a.

23. Drewnick, F.; Hings, S. S.; DeCarlo, P.; Jayne, J. T.; Gonin, M.; Fuhrer, K.; Weimer, S.; Jimenez, J. L.; Demerjian, K. L.; Borrmann, S.; Worsnop, D. R., A new time-of-flight aerosol mass spectrometer (TOF-AMS) - Instrument description and first field deployment. *Aerosol Sci. Technol.* **2005,** *39*, (7), 637-658.

24. Taira, M.; Kanda, Y., Continuous generation system for low-concentration gaseous nitrous acid. *Anal. Chem.* **1990,** *62*, (6), 630-633.

25. Jordan, A.; Haidacher, S.; Hanel, G.; Hartungen, E.; Märk, L.; Seehauser, H.; Schottkowsky, R.; Sulzer, P.; Märk, T. D., A high resolution and high sensitivity proton-transfer-reaction time-of-flight mass spectrometer (PTR-TOF-MS). *Int. J. Mass Spectrom.* **2009,** *286*, (2–3), 122-128.

26. Barmet, P.; Dommen, J.; DeCarlo, P. F.; Tritscher, T.; Praplan, A. P.; Platt, S. M.; Prévôt, A. S. H.; Donahue, N. M.; Baltensperger, U., OH clock determination by proton transfer reaction mass spectrometry at an environmental chamber. *Atmos. Meas. Tech.* **2012,** *5*, (3), 647-656.

27. Friedel, R. A.; Sharkey, A. G.; Shultz, J. L.; Humbert, C. R., Mass Spectrometric Analysis of Mixtures Containing Nitrogen Dioxide. *Anal. Chem.* **1953,** *25*, (9), 1314-1320.

28. Friedel, R. A.; Shultz, J. L.; Sharkey Jr, A. G., Mass spectrum of nitric acid. *Anal. Chem.* **1959,** *31*, (6), 1128.

29. Wang-Hansen, C.; Soltani, S.; Andersson, B., Kinetic Analysis of O2- and NO2-Based Oxidation of Synthetic Soot. *The Journal of Physical Chemistry C* **2013,** *117*, (1), 522-531.

30. Stanmore, B. R.; Tschamber, V.; Brilhac, J. F., Oxidation of carbon by NOx, with particular reference to NO2 and N2O. *Fuel* **2008,** *87*, (2), 131-146.

31. Prince, A. P.; Wade, J. L.; Grassian, V. H.; Kleiber, P. D.; Young, M. A., Heterogeneous reactions of soot aerosols with nitrogen dioxide and nitric acid: Atmospheric chamber and Knudsen cell studies. *Atmos. Environ.* **2002,** *36*, (36-37), 5729-5740.

32. Zouaoui, N.; Labaki, M.; Jeguirim, M., Diesel soot oxidation by nitrogen dioxide, oxygen and water under engine exhaust conditions: Kinetics data related to the reaction mechanism. *C. R. Chim.* **2014,** *17*, (7-8), 672-680.

33. Mehring, M.; Elsener, M.; Kröcher, O., Diesel soot catalyzes the selective catalytic reduction of NOx with NH3. *Top. Catal.* **2013,** *56*, (1-8), 440-445.

34. Mehring, M.; Elsener, M.; Kröcher, O., Selective catalytic reduction of NOx with ammonia over soot. *ACS Catal.* **2012,** *2*, (7), 1507-1518.

35. Atribak, I.; Bueno-López, A.; García-García, A., Uncatalysed and catalysed soot combustion under NOx+O2: Real diesel versus model soots. *Combust. Flame* **2010,** *157*, (11), 2086-2094.

36. NIST, http://webbook.nist.gov/cgi/cbook.cgi?ID=C124389&Mask=200#Mass-Spec.

37. Messerer, A.; Niessner, R.; Pöschl, U., Comprehensive kinetic characterization of the oxidation and gasification of model and real diesel soot by nitrogen oxides and oxygen under engine exhaust conditions: Measurement, Langmuir-Hinshelwood, and Arrhenius parameters. *Carbon* **2006,** *44*, (2), 307-324.

38. Goodman, A. L.; Underwood, G. M.; Grassian, V. H., A laboratory study of the heterogeneous reaction of nitric acid on calcium carbonate particles. *J. Geophys. Res. D Atmos.* **2000,** *105*, (D23), 29053-29064.

39. Leistner, K.; Nicolle, A.; Da Costa, P., Detailed kinetic analysis of soot oxidation by NO 2, NO, and NO + O 2. *Journal of Physical Chemistry C* **2012,** *116*, (7), 4642-4654.

40. Lanz, V. A.; Prévôt, A. S. H.; Alfarra, M. R.; Weimer, S.; Mohr, C.; Decarlo, P. F.; Gianini, M. F. D.; Hueglin, C.; Schneider, J.; Favez, O.; D'Anna, B.; George, C.; Baltensperger, U., Characterization of aerosol chemical composition with aerosol mass spectrometry in Central Europe: An overview. *Atmos. Chem. Phys.* **2010,** *10*, (21), 10453-10471.
41. Zotter, P.; Ciobanu, V. G.; Zhang, Y. L.; El-Haddad, I.; Macchia, M.; Daellenbach, K. R.; Salazar, G. A.; Huang, R. J.; Wacker, L.; Hueglin, C.; Piazzalunga, A.; Fermo, P.; Schwikowski, M.; Baltensperger, U.; Szidat, S.; Prévôt, A. S. H., Radiocarbon analysis of elemental and organic carbon in Switzerland during winter-smog episodes from 2008 to 2012-Part 1: Source apportionment and spatial variability. *Atmos. Chem. Phys.* **2014,** *14*, (24), 13551-13570.
42. Putaud, J. P.; Van Dingenen, R.; Alastuey, A.; Bauer, H.; Birmili, W.; Cyrys, J.; Flentje, H.; Fuzzi, S.; Gehrig, R.; Hansson, H. C.; Harrison, R. M.; Herrmann, H.; Hitzenberger, R.; Hüglin, C.; Jones, A. M.; Kasper-Giebl, A.; Kiss, G.; Kousa, A.; Kuhlbusch, T. A. J.; Löschau, G.; Maenhaut, W.; Molnar, A.; Moreno, T.; Pekkanen, J.; Perrino, C.; Pitz, M.; Puxbaum, H.; Querol, X.; Rodriguez, S.; Salma, I.; Schwarz, J.; Smolik, J.; Schneider, J.; Spindler, G.; ten Brink, H.; Tursic, J.; Viana, M.; Wiedensohler, A.; Raes, F., A European aerosol phenomenology - 3: Physical and chemical characteristics of particulate matter from 60 rural, urban, and kerbside sites across Europe. *Atmos. Environ.* **2010,** *44*, (10), 1308-1320.
43. Putaud, J. P.; Raes, F.; Van Dingenen, R.; Brüggemann, E.; Facchini, M. C.; Decesari, S.; Fuzzi, S.; Gehrig, R.; Hüglin, C.; Laj, P.; Lorbeer, G.; Maenhaut, W.; Mihalopoulos, N.; Müller, K.; Querol, X.; Rodriguez, S.; Schneider, J.; Spindler, G.; Ten Brink, H.; Tørseth, K.; Wiedensohler, A., A European aerosol phenomenology - 2: Chemical characteristics of particulate matter at kerbside, urban, rural and background sites in Europe. *Atmos. Environ.* **2004,** *38*, (16), 2579-2595.
44. Van Dingenen, R.; Raes, F.; Putaud, J. P.; Baltensperger, U.; Charron, A.; Facchini, M. C.; Decesari, S.; Fuzzi, S.; Gehrig, R.; Hansson, H. C.; Harrison, R. M.; Hüglin, C.; Jones, A. M.; Laj, P.; Lorbeer, G.; Maenhaut, W.; Palmgren, F.; Querol, X.; Rodriguez, S.; Schneider, J.; Ten Brink, H.; Tunved, P.; Tørseth, K.; Wehner, B.; Weingartner, E.; Wiedensohler, A.; Wåhlin, P., A European aerosol phenomenology - 1: Physical characteristics of particulate matter at kerbside, urban, rural and background sites in Europe. *Atmos. Environ.* **2004,** *38*, (16), 2561-2577.
45. Platt, S. M.; El-Haddad, I.; Zardini, A. A.; Clairotte, M.; Astorga, C.; Wolf, R.; Slowik, J. G.; Temime-Roussel, B.; Marchand, N.; Je\vz, ek, I.; Drinovec, L.; Mo\vc, nik, G.; M\"o, hler, O.; Richter, R.; Barmet, P.; Bianchi, F.; Baltensperger, U.; Pr\'e, v\; o, t, A. S. H., Secondary organic aerosol formation from gasoline vehicle emissions in a new mobile environmental reaction chamber. *Atmos. Chem. Phys.* **2013,** *13*, (18), 9141-9158.
46. Nordin, E. Z.; Eriksson, A. C.; Roldin, P.; Nilsson, P. T.; Carlsson, J. E.; Kajos, M. K.; Hellén, H.; Wittbom, C.; Rissler, J.; Löndahl, J.; Swietlicki, E.; Svenningsson, B.; Bohgard, M.; Kulmala, M.; Hallquist, M.; Pagels, J. H., Secondary organic aerosol formation from idling gasoline passenger vehicle emissions investigated in a smog chamber. *Atmos. Chem. Phys.* **2013,** *13*, (12), 6101-6116.
47. Tkacik, D. S.; Lambe, A. T.; Jathar, S.; Li, X.; Presto, A. A.; Zhao, Y.; Blake, D.; Meinardi, S.; Jayne, J. T.; Croteau, P. L.; Robinson, A. L., Secondary organic aerosol formation from in-use motor vehicle emissions using a potential aerosol mass reactor. *Environ. Sci. Technol.* **2014,** *48*, (19), 11235-11242.
48. Ng, N. L.; Canagaratna, M. R.; Jimenez, J. L.; Chhabra, P. S.; Seinfeld, J. H.; Worsnop, D. R., Changes in organic aerosol composition with aging inferred from aerosol mass spectra. *Atmos. Chem. Phys.* **2011,** *11*, (13), 6465-6474.
49. Bahreini, R.; Ervens, B.; Middlebrook, A. M.; Warneke, C.; de Gouw, J. A.; DeCarlo, P. F.; Jimenez, J. L.; Brock, C. A.; Neuman, J. A.; Ryerson, T. B.; Stark, H.; Atlas, E.; Brioude, J.; Fried, A.; Holloway, J. S.; Peischl, J.; Richter, D.; Walega, J.; Weibring, P.; Wollny, A. G.; Fehsenfeld, F. C., Organic aerosol formation in urban and industrial plumes near Houston and Dallas, Texas. *Journal of Geophysical Research-Atmospheres* **2009,** *114*.
50. Heeb, N. V.; Forss, A. M.; Brühlmann, S.; Lüscher, R.; Saxer, C. J.; Hug, P., Three-way catalyst-induced formation of ammonia-velocity- and acceleration-dependent emission factors. *Atmos. Environ.* **2006,** *40*, (31), 5986-5997.
51. Suarez-Bertoa, R.; Zardini, A. A.; Astorga, C., Ammonia exhaust emissions from spark ignition vehicles over the New European Driving Cycle. *Atmos. Environ.* **2014,** *97*, 43-53.
52. Hallquist, M.; Wenger, J. C.; Baltensperger, U.; Rudich, Y.; Simpson, D.; Claeys, M.; Dommen, J.; Donahue, N. M.; George, C.; Goldstein, A. H. H., J. F.; Herrmann, H.; Hoffmann, T.; Iinuma, Y.; Jang,

557 M.; Jenkin, M. E.; Jimenez, J. L.; Kiendler-Scharr, A.; Surratt, J. D.; Szmigielski, R.; Wildt, J., The
558 formation, properties and impact of secondary organic aerosol: current and emerging issues. *Atmos. Chem.*
559 *Phys.* **2009,** *9*, (14), 5155-5236.
560 53. Gupta, D.; Kim, H.; Park, G.; Li, X.; Eom, H. J.; Ro, C. U., Hygroscopic properties of NaCl and
561 NaNO3 mixture particles as reacted inorganic sea-salt aerosol surrogates. *Atmos. Chem. Phys.* **2015,** *15*,
562 (6), 3379-3393.
563 54. Williams, L. R.; Gonzalez, L. A.; Peck, J.; Trimborn, D.; McInnis, J.; Farrar, M. R.; Moore, K. D.;
564 Jayne, J. T.; Robinson, W. A.; Lewis, D. K.; Onasch, T. B.; Canagaratna, M. R.; Trimborn, A.; Timko, M.
565 T.; Magoon, G.; Deng, R.; Tang, D.; De La Rosa Blanco, E.; Prévôt, A. S. H.; Smith, K. A.; Worsnop, D.
566 R., Characterization of an aerodynamic lens for transmitting particles greater than 1 micrometer in diameter
567 into the Aerodyne aerosol mass spectrometer. *Atmos. Meas. Tech.* **2013,** *6*, (11), 3271-3280.
568 55. Weimer, S.; Alfarra, M. R.; Schreiber, D.; Mohr, M.; Prévôt, A. S. H.; Baltensperger, U., Organic
569 aerosol mass spectral signatures from wood-burning emissions: Influence of burning conditions and type. *J.*
570 *Geophys. Res. D Atmos.* **2008,** *113*, (10).
571 56. Calvo, A. I.; Martins, V.; Nunes, T.; Duarte, M.; Hillamo, R.; Teinilä, K.; Pont, V.; Castro, A.;
572 Fraile, R.; Tarelho, L.; Alves, C., Residential wood combustion in two domestic devices: Relationship of
573 different parameters throughout the combustion cycle. *Atmos. Environ.* **2015,** *116*, 72-82.

574

Figures

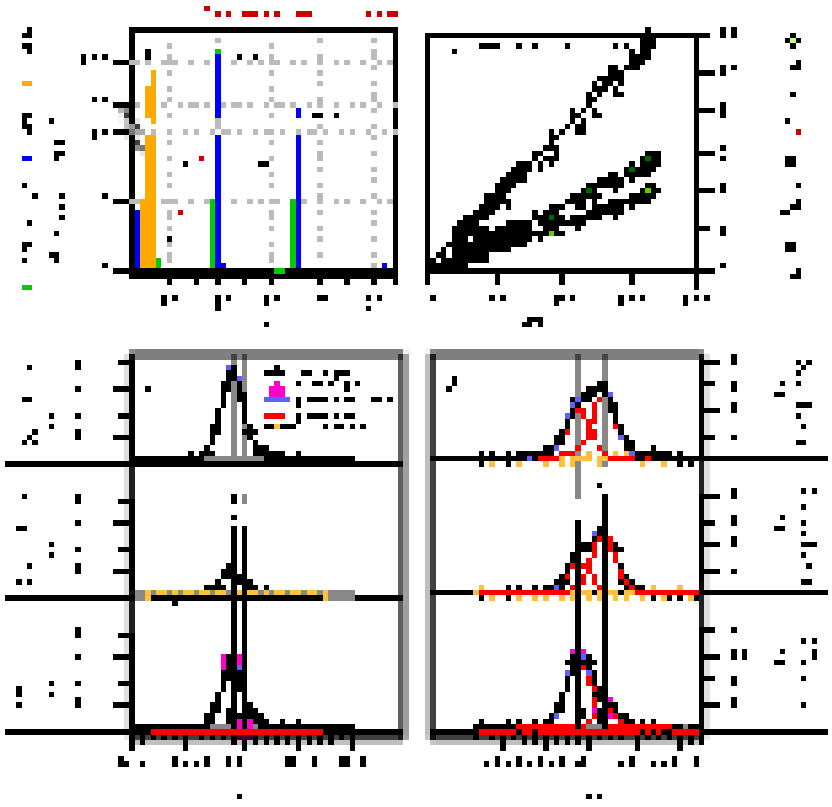

Figure 1. Observation of non-particle-bound CO_2^+ and CO^+ from NH_4NO_3 sampling. (a) HR-ToF-AMS mass spectrum of high purity NH_4NO_3 particles formed in a smog chamber from HNO_3 and NH_3 using standard fragmentation assumptions [12, 13] (HR3-Expt5): *m/z* 15 (NH^+), 16 (NH_2^+), 17 (NH_3^+), 30 (NO^+), 46 (NO_2^+) and 63 (HNO_3^+) are the main ions observed from NH_4NO_3 decomposition and fragmentation. Standard fragmentation assumptions are applied, i.e. N^+ (*m/z* 14) is assigned based on NO^+ and NO_2^+. CO_2^+ is observed at nominal *m/z* 44; organic *m/z* 18 (H_2O^+) and 28 (CO^+) are assigned based on CO_2^+.[12, 13] C^+ (*m/z* 12) is a measured EI fragment of CO_2^+. (b) CO_2^+ (nitrate eq. mass, RIE=1) and Org_{44} as well as the derived organic mass (standard fragmentation assumptions: $Org_{28}=Org_{44}*1$, $Org_{18}=Org_{44}*0.225$, $Org_{17}=Org_{44}*0.05625$ and $Org_{16}=Org_{44}*0.009$, gas phase CO_2 correction applied, RIE=1.4) scale proportionally with the NO_3 signal (RIE=1). Orthogonal distance linear fits are applied. (c) CO_2^+ signal as seen when particle beam is "*open*", "*closed*" and the calculated "*open-closed*" difference peak. Data were collected in synthetic air (N_2/O_2, free of gas phase CO_2) on instrument HR3. (d) CO^+ signal during NH_4NO_3 measurements performed in argon on instrument HR1. The N_2 signal arises from residual gas phase N_2 in the instrument background.

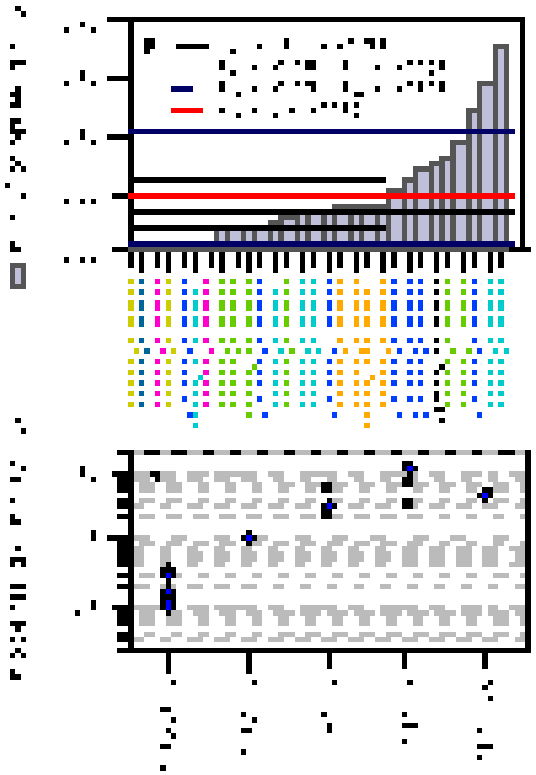

Figure 2. Variability in *k*. (a) The relationship *k* of CO_2^+ or *m/z* 44 and NO_3 signal (Hz or nitrate eq. mass, RIE=1) from NH_4NO_3 on 6 HR-ToF-AMS (HR1-6), 1 C-ToF-AMS and 1 Q-ACSM. The respective statistical parameters (median (i.e. 50^{th} percentile, P_{50}), 10^{th}, 25^{th}, 75^{th}, and 90^{th} percentile and average are given in the legend. The experiment date (YYYY/MM) is indicated on the axis labels. Experiment details and orthogonal distance linear fits are presented in Table S1 and Fig. S1. **(b)** Enhancement of *k* of CO_2^+ at *m/z* 44 vs the respective anion, i.e. NO_3 signal according to the summed signal of all ions attributed to NO_3 for all nitrate salts, SO_4 signal according to the summed signal of all ions attributed to SO_4 for $(NH_4)_2SO_4$[12, 13] ($RIE(SO_4)=1$, $RIE(NO_3)=1$), relative to *k* from NH_4NO_3 (experiments performed on HR1-3 and ACSM). Measurements were typically performed in CO_2-free synthetic air (N_2/O_2). All salts are tested at a vaporizer temperature of 600 °C, which is the typical setting during standard operation. Note, that KNO_3, $NaNO_3$ and $Ca(NO_3)_2$ do not fully vaporize at 600°C (see discussion in SI).

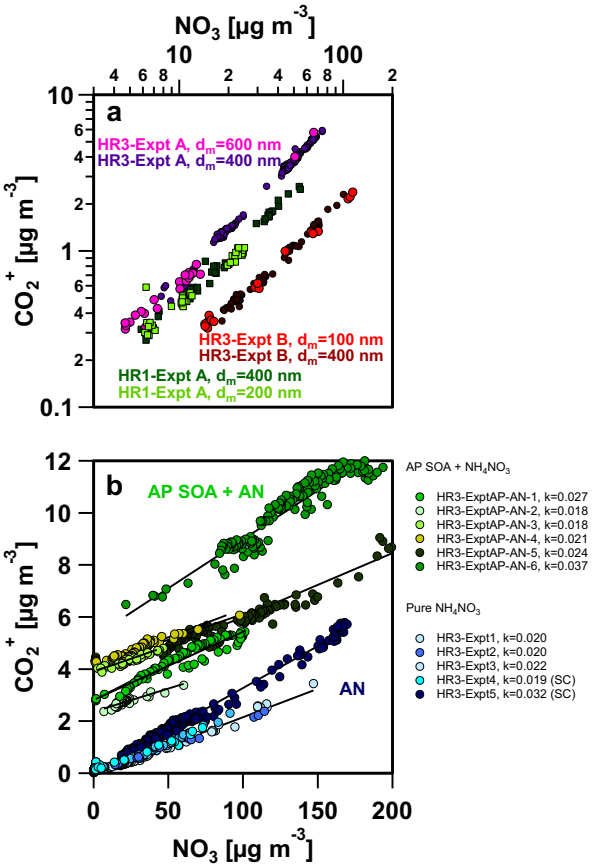

609

610 **Figure 3. Effect of particle diameter and mixing state. (a)** CO_2^+ signal induced at different
611 NH_4NO_3 particle diameter (HR1-Expt A, d_m=400 nm vs 100 nm, HR3-Expt A, d_m=400 vs 200 nm,
612 HR3-Expt B, d_m=400 vs 600 nm) **(b)** CO_2^+ signal from pure NH_4NO_3 particles (average
613 k=0.023±0.005) from nebulized salt solutions (HR3-Expt1,2,3) and generated in-situ in a SC from
614 gas phase precursors (HR3-Expt4 and 5) vs internally mixed particles of α-pinene (AP) SOA and
615 NH_4NO_3 (average k=0.024±0.007) (mixing state is given in SI) formed in a SC; estimated CO_2^+
616 enhancements based on changed CE are discussed in SI for mixed particles). Note that the intercept
617 in Fig. 3b represents the particulate CO_2^+ contained in AP SOA (at NH_4NO_3=0). The reader is also
618 referred to Fig. 4 for a typical SC experiment yielding the data in Fig. 3b. All data are presented as
619 nitrate eq. mass, i.e. RIE=1.

620

621

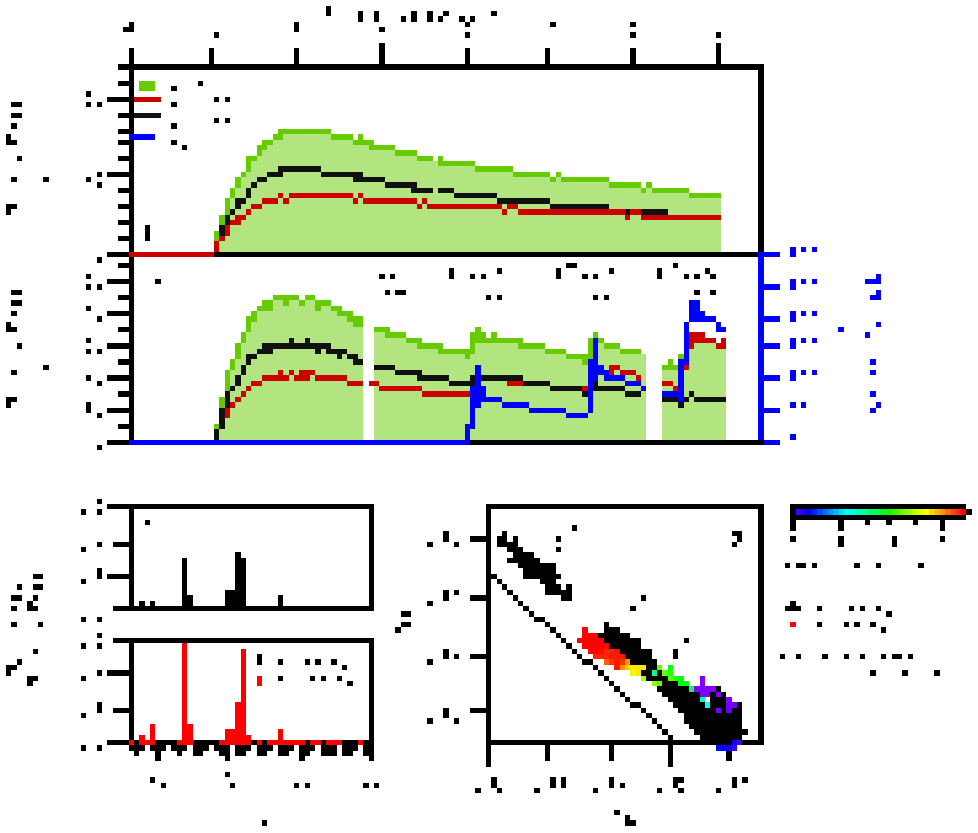

622

623 **Figure 4. *α*-pinene SOA at different ratios with NH_4NO_3 (a)** Reference experiment HR3-ExptAP-
624 2 w/o NH_4NO_3. **(b)** Smog chamber experiment HR3-ExptAP-AN-5 (k=0.025) (RIE=1.4 for OA
625 signals Org (organic), Org_{44} (organic mass at m/z 44, i.e. CO_2^+), Org_{43} (organic mass at m/z 43, i.e.
626 $C_2H_3O^+$) and RIE=1.1 for NO_3). Instrument settings and experiment conditions (AP and oxidant
627 concentrations) are given in Table S1. **(c-d)** Average mass spectrum with NH_4NO_3 at t=6h
628 compared to a reference AP SOA experiment w/o NH_4NO_3 (HR3-ExptAP-2). **(e)** f_{44}-f_{43} triangle
629 plots[15] for AP SOA experiments with NH_4NO_3 at NO_3/OA ratios of 1.7, 3.3 and 6.7 compared to
630 reference AP SOA experiments w/o NH_4NO_3 (HR3-ExptAP-2).

631

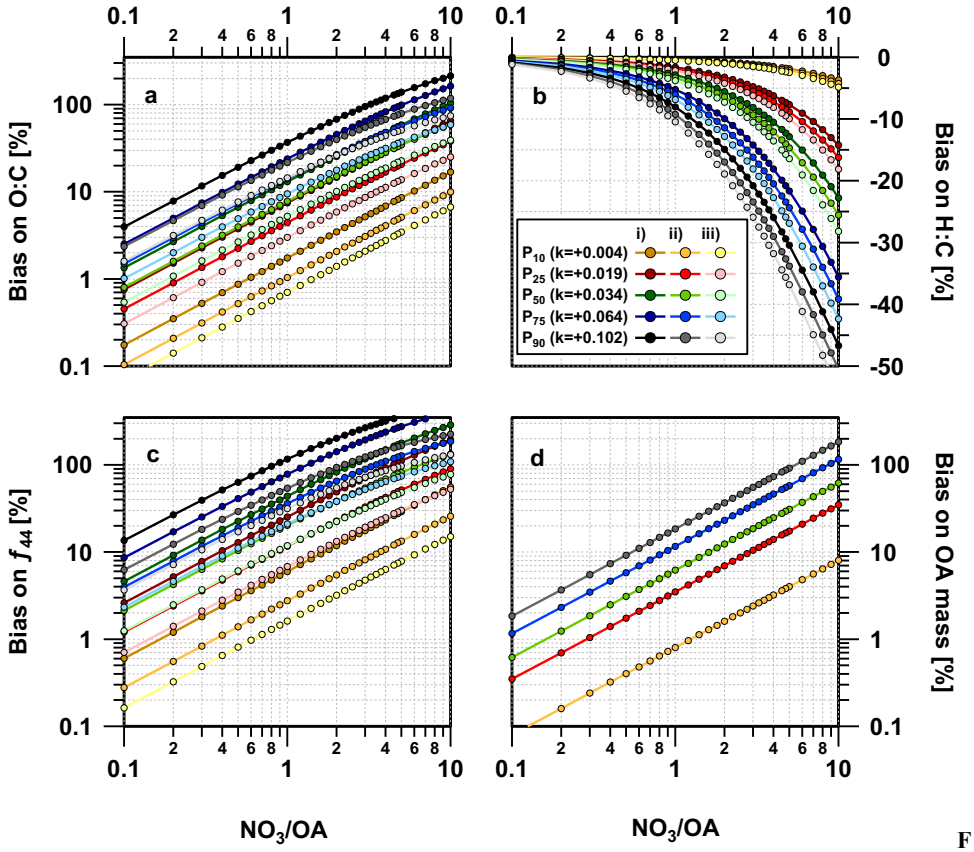

Figure 5. Bias estimation for the NH_4NO_3 induced interference on the (a) Oxygen-to-Carbon (O:C) and (b) Hydrogen-to-Carbon ratio (H:C), (c) fraction of organic *m/z* 44 to the total organic mass (f_{44}), and (d) OA mass. Percentiles ($P_{10\text{-}90}$) for *k* are based on Fig. 2a. The bias estimation assumes three scenarios for the true particle composition: (*i*) O:C=0.30, (*ii*) O:C=0.50, (*iii*) O:C=0.70, with H:C 1.5, and f_{44} and OM/OC based on Canagaratna et al.[14] (f_{44}=0.051, 0.098, 0.144; OM/OC=1.56, 1.82, 2.07). Standard fragmentation assumptions[12, 13] and RIE=1.4 for OA mass and 1.1 for NO_3 mass are applied when accounting for interferences on *m/z* 18 (H_2O^+) and 28 (CO^+) as well as *m/z* 17 (OH^+) and *m/z* 16 (O^+). Isotopes are not taken into account. The mixing ratio of NO_3 from NH_4NO_3 to OA is 0.1-1 for ambient data including winter times[3, 40-44] and 1-10 for e.g. studies investigating gasoline exhaust ageing[46, 47] .